An apolipoprotein-enriched biomolecular corona switches the cellular uptake mechanism and trafficking pathway of lipid nanoparticles

Luca Digiacomo,[a,b#] Francesco Cardarelli,[c#] Daniela Pozzi,[a] Sara Palchetti,[a] Michelle A. Digman,[d] Enrico Gratton,[d] Aldo Laganà,[g] Morteza Mahmoudi,[e,f *] Giulio Caracciolo[a*]

[a]*Department of Molecular Medicine, Sapienza University of Rome, Viale Regina Elena 291, 00161 Rome, Italy*

[b]*Department of Bioscience and Biotechnology, University of Camerino, Via Gentile III da Varano, 62032 Camerino, (MC), Italy*

[c]*NEST, Istituto Nanoscienze, CNR and Scuola Normale Superiore, Piazza San Silvestro 12, Pisa, Italy*

[d]*Laboratory for Fluorescence Dynamics, Biomedical Engineering Department, University of California Irvine, CA 92697, USA*

[e]*Department of Anesthesiology, Brigham and Women's Hospital, Harvard Medical School, Boston, MA 02115, USA*

[f]*Nanotechnology Research Centre, Faculty of Pharmacy, Tehran University of Medical Sciences, Tehran 13169-43551, Iran*

[g] *Department of Chemistry, Sapienza University of Rome, P.le Aldo Moro 5, 00185 Rome, Italy*

# These authors contributed equally

* Mmahmoudi@bwh.harvard.edu, giulio.caracciolo@uniroma1.it

ABSTRACT

It is now well accepted that, following exposure to biological milieus (e.g. after systemic administration), nanoparticles (NPs) get covered by an outer biomolecular corona (BC) that defines many of their biological outcomes, such as the elicited immune response, biodistribution, and targeting capabilities. In spite of this, the BC role in regulating the cellular uptake and the subcellular trafficking properties of NPs has remained elusive. Here we tackle this issue by employing multicomponent (MC) lipid NPs, human plasma (HP) and HeLa cells as models for nanoformulation, biological fluid and target cell, respectively. By confocal fluorescence microscopy experiments and image correlation analyses we quantitatively demonstrate that the BC promotes a neat switch of cell entry mechanism and subsequent intracellular trafficking, from macropinocytosis to clathrin-dependent endocytosis. Nano liquid chromatography tandem mass spectrometry identifies Apolipoproteins as the most abundant components of the BC tested here. Interestingly, this class of proteins can be target of LDL receptors, which in turn are abundant clathrin-enriched membrane domains. Our results highlight the crucial role of BC as an intrinsic trigger of specific NP-cell interactions and biological responses and set the basis for a rational exploitation of the BC for targeted delivery.

INTRODUCTION

In the last decades, nanoparticle (NP)-based delivery systems have been extensively studied and employed as for therapeutic purposes [1-7]. Many of the proposed solutions provide safe and efficient delivery of pharmaceutical nanoformulations to targeted cells and/or tissues. However, despite recent progresses and great expectations, few nanoformulations have reached clinical practice[6]. Such a wide gap between NP-based systems and advanced medicinal products was demonstrated to depend mainly on what occurs to NPs upon contact with a physiological environment (e.g. blood, interstitial fluids, saliva etc.).[8] Under *in vivo* conditions, in fact, NPs get covered by an outer biomolecular corona (BC), which changes their "synthetic identity" (i.e. size, surface charge, aggregation state etc.)[9]. It is precisely this new identity, usually referred to as "biological identity", which controls the biological fate of NPs, including their circulation time, immune system activation, accumulation in liver and spleen, removal from the bloodstream via the mononuclear phagocytic system (MPS), biodistribution and cellular interactions[7]. Concerning these latter in particular, since the function of nanomaterials is expected to be carried out in a specific cellular location,[10-11] accurate characterization of BC[12] and understanding NP-BC-cell interactions is a critical step to design safer and more efficient NPs as well as to predict possible toxicity effects[13-16]. After cellular association, most nanomaterials get internalized via endocytic pathways[17-19]. Some of them, such as clathrin-mediated endocytosis, are regulated by activation of transmembrane receptors, which activate intracellular signaling cascades that, in turn, control cellular processes such as cellular differentiation, proliferation and survival[10]. Some other, such as micropinocytosis, entail a series of events initiated by extensive plasma membrane reorganization or ruffling to form an external macropinocytic structure that is then enclosed and internalized[20]. It thus appears crucial to understand if BC plays a role in mediating the interaction of NPs with cell machinery.

To fulfill this gap, in this work, we explored cellular uptake, endocytic pathways and intracellular dynamics of NPs in HeLa cells, both in absence and presence of BC from human plasma (HP). We used multicomponent (MC) liposomes, in light of their proved high performances and potential applicability in a number of diseases[17, 21-23]. We focused on clathrin-mediated endocytosis (CME), caveolin-mediated endocytosis (CAV) and macropinocytosis (MCR) and detected significant differences between bare systems and NP-BC complexes. To evaluate the internalization mechanism of MC lipid NPs, we carried out fluorescence colocalization studies on two-channel images, then measured overlap and correlation of the signals corresponding to NPs and endocytic vesicles. Furthermore, we categorized the cytoplasmatic dynamics of the vesicles, by processing fluorescence image time-series. More precisely, we employed the iMSD method[24], i.e. a fluorescence-based spatiotemporal fluctuation analysis that makes possible to detect the mode of motion of vesicles from

imaging, in the form of a mean square displacement (MSD) versus time-delay plot. By coupling results from colocalization studies and intracellular dynamics experiments, here we claim that the BC is responsible for a switch in the internalization processes of lipid NPs and affects their intracellular trafficking mechanisms. Clearly, results of the present investigation cannot fully account for the complexity of the in vivo NP-BC-cellular interactions. To achieve this, comprehensive studies entailing libraries of NPs, BCs, and cells will be needed. However, we believe that basic studies like this will contribute to the design of specific targeted nanoformulations to exploit specific cellular pathways of interest. In this way, many off-target effects could be minimalized or even fully avoided.

RESULTS AND DISCUSSION

The use of NPs offers more effective solutions to a wide range of biomedical issues[25]. Their entry into target cells is a fundamental step towards boosting therapeutic efficacy. Upon contact with biological fluids, the surface of NPs is modified by the adsorption of biomolecules leading to formation of the so-called BC[6]. Key interactions are controlled by biomolecules residing at the interface between the NP surface and the biological target. It is well-known that understanding how this BC could affect the NP-interactions is more important than studying each entity (i.e. NPs and cells) individually[7]. Detailed knowledge of the parameters regulating these interactions could help to manipulate the physiochemical properties of NPs in order to dictate selective accumulation in certain locations (e.g. tissues, organs, etc.) or to promote tunable cellular interactions. Even tough recent literature suggests a strong relationship between the nature of BC and the NP-cell association[13-14, 26-27], its precise role in regulating cellular uptake and subcellular processes has not been identified yet. The central aim of this investigation was therefore to explore the role played by the BC on the cellular uptake and intracellular trafficking of NPs. MC liposomes exhibited significantly greater delivery efficiency in many cell lines as compared to commercially available formulations[17] and were therefore used as a reference. Usually, a preliminary characterization of lipid NPs both before and after exposure to plasma proteins provides information about the impact of the BC on the chemical physical properties of the employed systems. In this regard, we characterized MC liposomes and MC liposome-BC complexes in terms of size and Zeta potential. We found that bare liposomes have mean hydrodynamic diameter of about 145 nm and positive Zeta potential (35 mV). Following 1-hour exposure to HP, we detected a slight increase in particle size (180 nm) and the inversion of surface charge (Zeta potential = - 18 mV)[1]. Size enlargement is in agreement with the results of recent investigations showing that the liposome–BC is roughly 30-80 nm thick depending on the lipid composition[28], while ‘normalization’ of zeta potential has been frequently observed, given that most plasma proteins have a net negative charge at physiological pH[29]. Then, we administered liposomes

and liposome-BC complexes to HeLa cells to evaluate cytotoxicity and cell uptake by MTT assay and flow cytometry, respectively. Results are listed in Table 1. Following administration, the percentage of living cells was extremely high for both liposomes and liposome-BC complexes. This finding ensured good cytocompatibility of the employed systems. A similar trend was found in the outcomes of flow cytometry analysis, which quantifies the cell uptake as percentage of fluorescence cells. Measured values read 99% for bare liposomes and 93% for liposome-BC complexes. To investigate the role of BC on the cellular uptake and intracellular trafficking of MC liposomes we applied fluorescence microscopy that provides useful tools to quantify spatial distributions of labeled objects within living cells and their intracellular motion. By fluorescence colocalization experiments we measured overlap and correlation of the fluorescence signals arising from red-labeled particles and green-labeled endocytic vesicles, aiming at elucidating the possible impact of the BC on the internalization mechanisms of the employed NPs. Figure 1 shows some representative dual-color images depicting the colocalization of liposomes and liposome-BC complexes with endocytic vesicles, corresponding to clathrin-mediated endocytosis (CME), caveolae-mediated endocytosis (CAV) and macropinocytosis (MCR). Data processing is based on the evaluation of Manders and Pearson's coefficients (i.e. M_1, M_2 and P, respectively) whose measured values are reported in a comprehensive 3D scatter plot (Figure 1 panels D, E, F). To the sake of clarity, the superiority of Manders vs. Pearson's coefficients is under debate[30]. As establishing a ranking between Manders and Pearson's coefficients is beyond our scopes, we decided to calculate and report all of them. In this representation, each data point corresponds to a dual-color image and points belonging to the same class define a specific "cluster", i.e. a multivariate distribution that is uniquely characterized by average and covariance matrix. Interestingly, for CME and MCR, the distributions of liposome-BC complexes are clearly distinguishable with respect to those of bare liposomes (Figure 1 panels D, F). Colocalization of liposome-BC complexes with CME-vesicles yields higher values of all the coefficients, with respect to their bare counterparts (i.e. pristine MC liposomes). Projections along the coordinate axes are reported to compare all the measured values of M_1 (Figure 1 panel G), M_2 (Figure 1 panel H) and P (Figure 1 panel I). Of note, this trend is inverted for colocalization experiments with MCR-vesicles. By contrast, colocalization with CAV-vesicles yields almost superimposed distributions (Figure 1 panel E). Indeed, no significant difference is found for the colocalization parameters of liposome and liposome-BC complexes with CAV-vesicles. In summary, confocal imaging inspection followed by quantitative colocalization assays clarified that the cell entry of MC liposomes occurs mainly through MCR, while both clathrin- and caveolae-mediated endocytosis play a minor role in the process. This result is in very good agreement with previous findings by some of us[17]. MCR is a pinocytosis process resulting in the formation of large vesicles of

irregular size and shape, generated by actin-driven invagination of the plasma membrane[10]. This suggests that the cellular uptake of bare MC liposomes does not involve the utilization of lipid rafts or pit-forming proteins. Of note, BC clearly induces a switch in the mechanism of internalization of MC liposomes, from MCR to CME. This is noteworthy, as these clathrin-enriched domains cover a minor fraction of the cell surface (typically between 0.5–2%)[10]. Recently, it became clear that the mechanism of intracellular trafficking of NPs is crucial to sort components of the endocytic pathway to a number of subcellular destinations.

Motion characterization at intracellular level requires acquisition and post-processing of time series exploring the behavior of the investigated particles at high spatial and temporal resolution. In this regard, confocal microscopy and spatiotemporal image correlation analysis allowed us to categorize the intracellular dynamics of liposomes and liposome-BC complexes. In detail, we acquired fluorescence image-stacks (technical details are reported in the Methods section) and processed them through the *i*MSD method[24] that allowed us to categorize the particle mode of motion (Brownian diffusion vs. active transportation) and determine the main system's dynamic parameters, i.e. diffusion coefficient (D) and speed (v) of particles. The measured values of D and v for bare liposomes and liposome-BC complexes are reported in Figure 2 panel A, where each data point corresponds to an image time-series and ellipses describe the 2D distributions in terms of average values and covariance matrices. Distributions are located and oriented in distinct regions of the (D, v)-space, revealing significant differences between the intracellular dynamics of the investigated systems. Particularly, *i*MSD shows that bare liposomes are actively transported in the cytosol, while liposome-BC complexes mainly undergo Brownian diffusion (see supplementary Figure S1 for details). Similarly, we carried out iMSD analyses on CME, CAV and MCR vesicles. Measured values of the dynamic parameters are reported in Figure 2 panel B, which depicts the experimental data as 2D multivariate distributions. Dynamics of MCR vesicles (mainly active transport) is remarkably different as compared to that of, CME (mainly Brownian diffusion). Of note, a global comparison of these outcomes suggests that the intracellular dynamics of bare liposomes is similar to that of MCR vesicles as well as the motion of liposome-BC complexes resembles that of CME-vesicles, in keeping with colocalization results. These trends can be also recognized in the 1D distributions of diffusion coefficient (Figure 2 panel C) and particle speed (Figure 2 panel D). To provide quantitative estimation of this behavior, we compared multivariate distributions of NPs and endocytic vesicles in terms of Mahalanobis distance[31-32]. The Mahalanobis distance, here referred to as λ_M, is a statistical parameter representing a non-Euclidean distance between a data point and a distribution. In the employed representation, λ_M-values anisotropically increase from the average position of the 2D distribution, where $\lambda_M = 0$. Points on the ellipse have $\lambda_M = 1$ and $\lambda_M > 1$ outside the ellipse. Notably,

the statistical significance of the difference between $\lambda_M = 1$ and $\lambda_M = 2$ is the same as that of a data point located at σ or 2σ far from the mean value of a normal distribution of variance σ^2. We report in Figure 3 panel A the measured λ_M between data points corresponding to liposomes and the distributions of endocytic vesicles. Results confirm that the dynamic parameters of liposomes are located "far" from the distribution of CME-vesicles (maximum $<\lambda_M>=1.95$) and "near" that of MCR-vesicles (minimum $<\lambda_M>=1.01$). This trend is inverted for liposome-BC complexes (Figure 3 panel B).

In summary, our body of evidence shows that: i) pristine liposomes are mainly internalized by MCR and, once inside HeLa cells, their mode of motion resembles that of macropinosomes (active transportation); ii) The preferential uptake pathway of liposome-BC complexes is CME and their intracellular trafficking is similar to that of CME-vesicles. Collectively, our data show that BC triggers favorable interactions of MC liposomes with clathrin-coated pits. CME, among others, has the function to regulate the mechanism by which cells achieve nutrients and plasma membrane components, such as cholesterol, via low-density lipoproteins (LDL) and vesicles containing proteins with receptor binding sites[10] While clarifying the exact molecular mechanisms regulating the internalization of liposome-BC complexes within HeLa cells is beyond the scope of this investigation, our findings are likely to suggest that some “corona proteins” may favorably interact with receptor molecules in turn internalized by CME. To verify this speculation, we characterized the BC of MC liposomes by liquid chromatography (LC) tandem mass spectrometry (MS/MS). Table 2 shows the 25 most abundant proteins identified in the BC (the full list of identified proteins is given in Table S1): interestingly, MC liposomes are mainly covered by apolipoproteins (Apo A-I, Apo C−II, Apo E, Apo C−III, Apo A−IV are the most enriched). Remarkably, it is well known that Apolipoproteins can be targets of the LDL receptor, which in turn is preferentially localized within clathrin-enriched domains. Our future biological understanding of how NPs interact with cells will confirm these conclusions more in depth by benefiting from a detailed knowledge of the arrangements of functional motifs of BC components at the nanoscale[34-36]. Figure 4 summarizes our present understanding of the role played by BC on the MC liposome association with HeLa cells. BC controls the mechanism of NP-cell association and directs the cellular uptake via specific internalization pathways, CME in our case. This is crucial point, since each internalization route has its own intracellular dynamics (i.e. fast vs. slow dynamics) and final fate. Thus, when one designs NPs for biomedical applications[37] the BC should be carefully considered, since it greatly influences the mechanism of cellular uptake and, in turn, the intracellular trafficking. Still, basic studies like this shall contribute to the design of specific nanodelivery systems to exploit specific endocytic pathways of interest. This aspect may have a dramatic application in the emerging field of “personalized nanomedicine”[38]. Some of us have shown

that alterations in concentration and structure of plasma proteins as those produced by clinical manifestations of disease lead to formation of "personalized BC" (PBC)[5, 39]. Among other implications, this means that various cell types may employ different pathways to internalize NPs with their own PBC. To dictate selective accumulation of NPs at the desired target site, comprehensive studies involving libraries of NPs, PBCs, and cell lines will be needed. In this way, many off-target effects that typically occur *in vivo* could be minimized or fully prevented.

CONCLUSIONS

For the first time here, we probe the role of BC in directing liposomes interaction with living cells. The switch from the synthetic identity (MC liposomes) to the biological one (MC liposomes with absorbed BC) is proved to be responsible for a neat switch in the uptake mechanism and intracellular trafficking properties of NPs, from macropinocytosis to clathrin-mediated endocytosis. Since Apolipoproteins are the main components of the BC, we suggest that this protein class may be active player in triggering receptor-mediated uptake of liposome-BC into HeLa cells. This finding sheds new light on the basic molecular determinants of NP interaction with living matter and, potentially, paves the way to a new era of studies aimed at creating targeted nanoformulations to exploit specific cellular pathways of interest. The knowledge obtained from this study will contribute to understand basic principles of the uptake mechanism. This will allow better predicting and controlling the biodistribution of liposomes, which could lead to engineer such nanomaterials for specific targeting of tissues and/or organs of interest.

METHODS

Human Plasma collection

Human whole blood was achieved from the Department of Experimental Medicine ('Sapienza' University of Rome) by venipuncture of healthy subjects aged 20–40 years, using BD TM P100 Blood Collection System (Franklin Lakes, NJ, USA) with anticoagulant (K_2EDTA) and protease inhibitors cocktail. After clot formation, blood samples were centrifugated at 1000xg for 5 min. After checking the absence of hemolysis, the supernatant was collected and pooled to reduce alterations between volunteers and decrease the inter-personal variation. Then, pooled plasma samples were aliquoted and stored at -80 °C in labeled Protein LoBind tubes to ensure plasma stability during storage. Before analysis, plasma samples were thawed at 4°C and then warmed at room temperature.

Preparation of liposomes

Cationic lipids (3β-[N-(N',N'-dimethyl\-aminoethane)-carbamoyl])-cholesterol (DC-Chol) and 1,2-Dioleoyl-3-trimethyl-ammonium-propane (DOTAP), zwitterionic lipids dioleoyl-phosphocholine (DOPC) and dioleoyl-phosphatidyl-ethanol-amine (DOPE) were purchased from Avanti Polar Lipids (Alabaster, AL) and used without further refinement. For the preparation of MC liposomes, DC-Chol, DOTAP, DOPC and DOPE were dissolved in chloroform (molar ratios 1:1:1:1) and the solvent was evaporated under vacuum for 2 hours. Lipid films were then hydrated with ultrapure water to obtain a final concentration of 1 mg/ml. Finally, the obtained liposome solutions were extruded 20 times through a 0.1 μm polycarbonate filter with an Avanti Mini-Extruder (Avanti Polar Lipids, Alabaster, AL). For fluorescence microscopy experiment liposomal formulations were synthesized with the addition of Texas red-DOPE (Life Technologies, Carlsbad, CA) (Concentration 7 10^{-3} mg/mL; fluorescent lipid/total lipid molar ratio = 5/1000).

Preparation of liposome-BC complexes

MC liposomes-BC complexes were obtained by incubating MC liposomes with human plasma (HP) for one hour at a fixed ratio of 1:1 v/v.

Characterization of complexes

A preliminary characterization of the complexes has been carried out in terms of hydrodynamic radius and zeta potential. All size and zeta potential measurements were made on a Zetasizer Nano ZS90 (Malvern, U.K.) equipped with a 5 mW HeNe laser (wavelength = 632.8 nm) and a digital logarithmic correlator. All the results are given as mean ± standard deviation of three independent replicates.

Cell culture

Human cervical cancer cell line (HeLa), derived from human cervix adenocarcinoma, was purchase from ATCC (Manassas, VA, USA). HeLa cells were maintained in Eagle's Minimum Essential Medium (EMEM) supplemented with 2 mM L-glutamine, 100 IU/mL penicillin/streptomycin, 1 mM sodium pyruvate, 10 mM hepes, 1.5 mg/L sodium bicarbonate and 10% fetal bovine serum (FBS).

Flow cytometry

To investigate cellular uptake of nanoparticles in HeLa cells, liposomal formulations were synthesized with the addition of Texas red-DOPE (Life Technologies, Carlsbad, CA) (Concentration 7 10^{-3} mg/mL; fluorescent lipid/total lipid molar ratio = 5/1000). Bare liposomes and liposome-HP complexes were administered to cells cultured with serum-free medium. HeLa cells were plated 200,000 cells/mL in 12-well dishes. After 24 hours, cells were incubated for 3 hours with 10 μg/mL

of Texas res-labeled liposomes in serum-free Optimem medium. After the treatment cells were detached with trypsin/ethylenediaminetetraacetic acid (EDTA), washed two times with cold PBS, and run on a BD LSFORTESSA (BD Biosciences, San Jose, CA, USA). Cells were gated using forward vs side scatter to exclude debris. Data were analyzed using FlowJo software (FlowJo LLC data analysis software, Ashland, OR, USA).

Cell viability

To evaluate the potential toxicity arising from the administration of NPs, cell viability of HeLa cells was assessed by 3-(4,5-dymethyl thiazol 2-y1)-2,5-diphenyl tetrazolium bromide (MTT, mitochondrial respiration analysis; Sigma-Aldrich), according to Mosmann protocol. Briefly, HeLa cells were seeded on 96-wells plate (10,000 cells/well). The day after, cells were treated with 10 g/mL of each formulation in Optimem medium (Life Technologies, Carlsbad, CA) for 24 hours. Then, MTT was added to each well at the final concentration of 0.5 mg/mL and after 4 hours of incubation at 37 °C, the formazan salt was dissolved with 100 μL isopropylic alcohol. The absorbance of each well was measured with Glomax Discover System (Promega, Madison, WI, USA), a ready-to-use high performance multimode detection instrument.

Colocalization analysis

Fluorescence colocalization experiments were performed with an Olympus FV1000 (Olympus, Tokyo, Japan) confocal microscope (objective: 60x, 1.40 NA, oil-immersion), equipped with an X-light spinning disk (pinhole aperture: 70 μm) and Lumencor Spectra X-LED illumination. Hela cells were seeded onto 12 mm round glass coverlips and incubated for 1h in Optimem medium. MC liposomes and MC liposome-BC complexes were labeled with Texas red-DOPE (excitation/emission wavelengths: 595/615 nm). Lysosomes, clathrin, caveolae and macropinosomes were labeled with lysotracker, transferrin, cholera-toxin and dextran fluorescent dyes, respectively (excitation/emission wavelengths: 495/519 nm). Measurements of colocalization are based on the evaluation of Pearson's and Manders coefficients[40-41] of dual-color fluorescence images, i.e. red (R) channel for complexes and green (G) channel for endocytic vesicles. The Pearson's coefficient measures statistic correlation between the detected intensities of the two channels and is defined as

$$P = \frac{\sum_k \left[(R_k - \langle R \rangle)^2 \times (G_k - \langle G \rangle)^2 \right]}{\sqrt{\sum_k \left[(R_k - \langle R \rangle)^2 \times (G_k - \langle G \rangle)^2 \right]}} \qquad (1)$$

where R_k and G_k refer to the intensity values of the k-th pixel from red and green channel respectively and the brackets indicate averaging operations over the entire image[42]. P values range from 1 (i.e. perfect linear correlation) to -1 (anticorrelation). Values near zero reflect distributions that are not correlated with one another. Manders coefficients M_1 and M_2 evaluate the overlap of the detected signals from the two channels. We carried out a pre-processing procedure according to the Costes method[42] to determine the threshold intensities, below which a pixel can be regarded as dark (i.e. with zero intensity). Thus, thresholds have been iteratively calculated and uniquely defined by the correlation of the raw channels. The Costes method is considered a robust and reproducible method that eliminates user bias and can be easily automated [42]. Finally, Manders coefficients have been obtained as[40, 42]:

$$M_1 = \frac{\sum_k R'_k}{\sum_k R_k} \qquad (2)$$

where $R_k'=R_k$ if $G_k>0$ and $R_k'=0$ if $G_k=0$ and

$$M_2 = \frac{\sum_k G'_k}{\sum_k G_k} \qquad (3)$$

where $G_k'=G_k$ if $R_k>0$ and $G_k'=0$ if $R_k=0$.

These split parameters quantify the percentage of not-dark pixels in both channels with respect to the total number of not-dark pixels in Channel R and Channel G, separately. Colocalization analyses were performed using Coloc2 plugin on ImageJ software (https://imagej.nih.gov/ij/).

Measurements of intracellular dynamics

To study the intracellular dynamics of complexes, fluorescence microscopy experiments were performed with an Olympus FV1000 (Olympus, Tokyo, Japan) confocal microscope (objective: 100x, 1.40 NA, oil-immersion), provided with an X-light spinning disk (pinhole aperture: 70 μm) and Lumencor Spectra X-LED illumination. To study the intracellular dynamics of endocytic vesicles, fluorescence microscopy experiments were performed with an Olympus FluoView FV1000 confocal microscope with a 60x NA 1.20 water immersion objective. All experiments were carried out at 37 °C and 5% CO_2 using an incubation chamber enclosing the microscope stage and body. The diameter of the detection pinhole was set to the size of 1 Airy. Sequential image series at 16 bits were collected at a fixed pixel size of 69 nm selecting a region of interest of 256x256 pixels and by varying the pixel

dwell time from 0.5 to 2 or 4 μs per pixel depending on the characteristic diffusivity of the structure under study. The overall acquisition time varied from 30 to 60 seconds. Image-stacks of at least 300 frames were collected at 1 Hz and the dynamics of about 7000 detected particles was determined by custom scripts working on MATLAB (MathWorks Inc., Natick, MA).

The processing is based on an image-derived mean square displacement method (iMSD)[24] which allowed us to characterize the investigated dynamics in terms of diffusion coefficient D and particle speed v. In detail, the approach is based on the evaluation of the spatiotemporal correlation function g of the fluorescence fluctuations δi, which are recorded pixel by pixel, frame by frame. g is defined as follows:

$$g(x,h,t) = \frac{\left\langle i(x,y,t)i(x+x,y+h,t+t)\right\rangle}{\left\langle i(x,y,t)\right\rangle^2} - 1 \qquad (4)$$

where ξ and η are the distance between correlated pixels in the x and y directions, respectively, τ is the time lag, i(x, y, t) is the fluorescence intensity at point (x, y) and time t, and <i(x,y,t)i(x+ξ,y+η,t+τ)> indicates the average over spatial and time variables x, y and t. [43-44] g(ξ,η,τ) fits to standard Gaussian functions, i.e.

$$g(x,h,t) = g_\infty + g_1(t)\exp\left\{-\frac{(x - v_x t)^2 + (h - v_h t)^2}{s^2(t)}\right\} \qquad (5)$$

where the numerator of the exponential term describes the net flux of particles along a specific direcion in terms of average velocity, i.e. $\left\langle \vec{v} \right\rangle = \vec{v}_\Phi \equiv (v_\xi ; v_\eta)$

$$s^2(t) = s_0^2 + 4Dt + v_s^2 t^2 \qquad (6)$$

Thus, through fitting procedures of the spatiotemporal correlation function, we determined diffusion coefficient D and speed v (as $v^2=v^2_\varphi + v^2_\sigma$) of lipid complexes and endocytic vesicles[24].

Protein Identification and Quantification.

MC liposomes (100 μL, concentration =1 mg/mL) were incubated with 100 μL of HP at 37 °C. After 1-h incubation, liposome−BC complexes were centrifuged (14,000 rpm for 15 min) to remove loosely bound proteins. Subsequently, pellets were washed three times with 100 μL of the dissolving buffer (Tris-HCl pH 7.4, 10 mmol L^{-1}; NaCl, 150 mmol L^{-1}; EDTA, 1 mmol L^{-1}). Protein denaturation,

digestion, and desalting were carried out by a robust methodology that is commonly used to separate liposome−BC complexes from unbound proteins[45]. Afterwards, lyophilization was performed by a Speed-Vac apparatus (mod. SC 250 Express; Thermo Savant, Holbrook, NY, USA). Then samples were reconstituted with 0.1% HCOOH solution (final concentration 0.32 mg/mL) and stored at - 80 °C until LC MS/MS was done .Tryptic peptides were examined by a nano-LC system (Dionex Ultimate 3000, Sunnyvale, CA, USA) connected to a hybrid mass spectrometer (Thermo Fisher Scientific Bremen, Germany), equipped with a nanoelectrospray ion source. Experimental details have been already reported.[45] Xcalibur (v.2.07, ThermoFisher Scientific) raw data files were submitted to Proteome Discover (1.2 version, Thermo Scientific) for database search using Mascot (version 2.3.2 Matrix Science). Data were searched against SwissProt database (v 57.15, 20 266 sequences) using the decoy search option of Mascot. Finally, protein quantification was made by Scaffold software. For each identified protein, the mean value of (normalized spectral countings, NSCs) was normalized to the protein molecular weight (MWNSC) to obtain the relative protein abundance (RPA). Statistical significance of data was guaranteed by replicating the procedure for nine samples (three technical replicates for three independent biological samples). Data of relative protein abundance were provided as mean ± standard deviation.

Table 1. Preliminary characterization of the liposomes both in the absence (i.e. bare Liposomes) and in the presence of the biomolecular corona (BC) (i.e. Liposome-BC), in terms of average hydrodynamic diameter, Zeta potential, cell viability and uptake on HeLa cells.

	Liposome	Liposome-BC
Particle size (nm)	144±4	178±6
Zeta potential (mV)	34.5±1.1	-30±2
Cell viability (%)	99±1	89±5
Cell uptake (%)	98.9±0.3	92.8±2.3

Table 2. List of the twenty five most abundant plasma proteins identified in the biomolecular corona of MC liposomes. Relative protein abundance (RPA) is the average of nine measurements ±elative protein abundance (RPA)

#	Identified Proteins	Accession Number	Molecular Weight (kDa)	RPA(%)	St. Dev. (%)
1	Apolipoprotein A-I	APOA1	31	2.69	0.07
2	Apolipoprotein C-II	APOC2	11	2.66	0.07
3	Apolipoprotein E	APOE	36	2.44	0.06
4	Apolipoprotein C-III	APOC3	11	2.37	0.05
5	Apolipoprotein A-IV	APOA4	45	2.22	0.05
6	Apolipoprotein C-I	APOC1	9	1.74	0.04
7	Apolipoprotein A-II	APOA2	11	1.67	0.04
8	Complement C3	CO3	187	1.66	0.04
9	Keratin, type II cytoskeletal 1	K2C1	66	1.50	0.04
10	Prothrombin	THRB	70	1.50	0.04
11	Complement C4-B	CO4B	193	1.47	0.04
12	Fibrinogen beta chain	FIBB	56	1.46	0.04
13	Tropomyosin alpha-4 chain	TPM4	29	1.44	0.04
14	Ig kappa chain C region	IGKC	12	1.38	0.03
15	Serum albumin	ALBU	69	1.35	0.04
16	Vitronectin	VTNC	54	1.29	0.03
17	Inter-alpha-trypsin inhibitor heavy chain H2	ITIH2	106	1.29	0.03
18	Transthyretin	TTHY	16	1.27	0.03
19	Hemoglobin subunit beta	HBB	16	1.26	0.04
20	Ig kappa chain V-III region HAH	KV312	14	1.24	0.03
21	Ig lambda-2 chain C regions	LAC2	11	1.23	0.03
22	Fibrinogen gamma chain	FIBG	52	1.21	0.03
23	Keratin, type I cytoskeletal 9	K1C9	62	1.19	0.03
24	Clusterin	CLUS	52	1.18	0.03
25	Fibrinogen alpha chain	FIBA	95	1.17	0.03

References

1. Caracciolo, G., Liposome–protein corona in a physiological environment: Challenges and opportunities for targeted delivery of nanomedicines. *Nanomedicine: Nanotechnology, Biology and Medicine* **2015,** *11* (3), 543-557.
2. Docter, D.; Westmeier, D.; Markiewicz, M.; Stolte, S.; Knauer, S.; Stauber, R., The nanoparticle biomolecule corona: lessons learned–challenge accepted? *Chemical Society reviews* **2015,** *44* (17), 6094-6121.
3. Mahmoudi, M.; Sheibani, S.; Milani, A. S.; Rezaee, F.; Gauberti, M.; Dinarvand, R.; Vali, H., Crucial role of the protein corona for the specific targeting of nanoparticles. *Nanomedicine* **2015,** *10* (2), 215-226.
4. Maiolo, D.; Del Pino, P.; Metrangolo, P.; Parak, W. J.; Baldelli Bombelli, F., Nanomedicine delivery: does protein corona route to the target or off road? *Nanomedicine* **2015,** *10* (21), 3231-3247.
5. Corbo, C.; Molinaro, R.; Parodi, A.; Toledano Furman, N. E.; Salvatore, F.; Tasciotti, E., The impact of nanoparticle protein corona on cytotoxicity, immunotoxicity and target drug delivery. *Nanomedicine* **2016,** *11* (1), 81-100.
6. Caracciolo, G.; Farokhzad, O. C.; Mahmoudi, M., Biological Identity of Nanoparticles In Vivo: Clinical Implications of the Protein Corona. *Trends in Biotechnology* **2017,** *35* (3), 257-264.
7. Polo, E.; Collado, M.; Pelaz, B.; del Pino, P., Advances toward More Efficient Targeted Delivery of Nanoparticles in Vivo: Understanding Interactions between Nanoparticles and Cells. *ACS nano* **2017,** *11* (3), 2397-2402.
8. Salvati, A.; Pitek, A. S.; Monopoli, M. P.; Prapainop, K.; Bombelli, F. B.; Hristov, D. R.; Kelly, P. M.; Åberg, C.; Mahon, E.; Dawson, K. A., Transferrin-functionalized nanoparticles lose their targeting capabilities when a biomolecule corona adsorbs on the surface. *Nature nanotechnology* **2013,** *8* (2), 137-143.
9. Walkey, C. D.; Chan, W. C. W., Understanding and controlling the interaction of nanomaterials with proteins in a physiological environment. *Chemical Society Reviews* **2012,** *41* (7), 2780-2799.
10. Behzadi, S.; Serpooshan, V.; Tao, W.; Hamaly, M. A.; Alkawareek, M. Y.; Dreaden, E. C.; Brown, D.; Alkilany, A. M.; Farokhzad, O. C.; Mahmoudi, M., Cellular uptake of nanoparticles: journey inside the cell. *Chemical Society Reviews* **2017**.
11. Di Silvio, D.; Maccarini, M.; Parker, R.; Mackie, A.; Fragneto, G.; Bombelli, F. B., The effect of the protein corona on the interaction between nanoparticles and lipid bilayers. *Journal of Colloid and Interface Science* **2017**.
12. Carrillo-Carrion, C.; Carril, M.; Parak, W. J., Techniques for the experimental investigation of the protein corona. *Current Opinion in Biotechnology* **2017,** *46*, 106-113.
13. Walkey, C. D.; Olsen, J. B.; Song, F.; Liu, R.; Guo, H.; Olsen, D. W. H.; Cohen, Y.; Emili, A.; Chan, W. C., Protein corona fingerprinting predicts the cellular interaction of gold and silver nanoparticles. *ACS nano* **2014,** *8* (3), 2439-2455.
14. Liu, R.; Jiang, W.; Walkey, C. D.; Chan, W. C.; Cohen, Y., Prediction of nanoparticles-cell association based on corona proteins and physicochemical properties. *Nanoscale* **2015,** *7* (21), 9664-9675.
15. Sahneh, F. D.; Scoglio, C. M.; Monteiro-Riviere, N. A.; Riviere, J. E., Predicting the impact of biocorona formation kinetics on interspecies extrapolations of nanoparticle biodistribution modeling. *Nanomedicine* **2015,** *10* (1), 25-33.
16. Treuel, L.; Docter, D.; Maskos, M.; Stauber, R. H., Protein corona–from molecular adsorption to physiological complexity. *Beilstein journal of nanotechnology* **2015,** *6* (1), 857-873.
17. Pozzi, D.; Marchini, C.; Cardarelli, F.; Rossetta, A.; Colapicchioni, V.; Amici, A.; Montani, M.; Motta, S.; Brocca, P.; Cantù, L., Mechanistic understanding of gene delivery mediated by highly efficient multicomponent envelope-type nanoparticle systems. *Molecular pharmaceutics* **2013,** *10* (12), 4654-4665.
18. Ojeda, E.; Puras, G.; Agirre, M.; Zarate, J.; Grijalvo, S.; Eritja, R.; Digiacomo, L.; Caracciolo, G.; Pedraz, J. L., The role of helper lipids in the intracellular disposition and transfection efficiency of niosome formulations for gene delivery to retinal pigment epithelial cells. *International Journal of Pharmaceutics* **2016,** *503* (1-2), 115-126.

19. Rejman, J.; Bragonzi, A.; Conese, M., Role of clathrin- and caveolae-mediated endocytosis in gene transfer mediated by lipo- and polyplexes. *Molecular Therapy* **2005,** *12* (3), 468-474.
20. Swanson, J. A.; Watts, C., Macropinocytosis. *Trends in cell biology* **1995,** *5* (11), 424-428.
21. Caracciolo, G.; Pozzi, D.; Amenitsch, H.; Caminiti, R., Multicomponent cationic lipid-DNA complex formation: Role of lipid mixing. *Langmuir* **2005,** *21* (25), 11582-11587.
22. Caracciolo, G.; Pozzi, D.; Caminiti, R.; Amenitsch, H., Lipid mixing upon deoxyribonucleic acid-induced liposomes fusion investigated by synchrotron small-angle x-ray scattering. *Applied Physics Letters* **2005,** *87* (13), 1-3.
23. Palchetti, S.; Pozzi, D.; Marchini, C.; Amici, A.; Andreani, C.; Bartolacci, C.; Digiacomo, L.; Gambini, V.; Cardarelli, F.; Di Rienzo, C.; Peruzzi, G.; Amenitsch, H.; Palermo, R.; Screpanti, I.; Caracciolo, G., Manipulation of lipoplex concentration at the cell surface boosts transfection efficiency in hard-to-transfect cells. *Nanomedicine: Nanotechnology, Biology, and Medicine* **2017,** *13* (2), 681-691.
24. Digiacomo, L.; Digman, M. A.; Gratton, E.; Caracciolo, G., Development of an image Mean Square Displacement (iMSD)-based method as a novel approach to study the intracellular trafficking of nanoparticles. *Acta Biomaterialia* **2016,** *42*, 189-198.
25. Heath, J. R., Nanotechnologies for biomedical science and translational medicine. *Proceedings of the National Academy of Sciences* **2015,** *112* (47), 14436-14443.
26. Bigdeli, A.; Palchetti, S.; Pozzi, D.; Hormozi-Nezhad, M. R.; Baldelli Bombelli, F.; Caracciolo, G.; Mahmoudi, M., Exploring Cellular Interactions of Liposomes Using Protein Corona Fingerprints and Physicochemical Properties. *ACS nano* **2016,** *10* (3), 3723-3737.
27. Palchetti, S.; Digiacomo, L.; Pozzi, D.; Peruzzi, G.; Micarelli, E.; Mahmoudi, M.; Caracciolo, G., Nanoparticles-cell association predicted by protein corona fingerprints. *Nanoscale* **2016,** *8* (25), 12755-12763.
28. Caracciolo, G.; Pozzi, D.; Capriotti, A. L.; Cavaliere, C.; Piovesana, S.; La Barbera, G.; Amici, A.; Laganà, A., The liposome-protein corona in mice and humans and its implications for in vivo delivery. *Journal of Materials Chemistry B* **2014,** *2* (42), 7419-7428.
29. Caracciolo, G., Liposome-protein corona in a physiological environment: Challenges and opportunities for targeted delivery of nanomedicines. *Nanomedicine: Nanotechnology, Biology, and Medicine* **2015,** *11* (3), 543-557.
30. Adler, J.; Parmryd, I., Quantifying colocalization by correlation: the Pearson correlation coefficient is superior to the Mander's overlap coefficient. *Cytometry Part A* **2010,** *77* (8), 733-742.
31. De Maesschalck, R.; Jouan-Rimbaud, D.; Massart, D. L., The mahalanobis distance. *Chemometrics and intelligent laboratory systems* **2000,** *50* (1), 1-18.
32. Xiang, S.; Nie, F.; Zhang, C., Learning a Mahalanobis distance metric for data clustering and classification. *Pattern Recognition* **2008,** *41* (12), 3600-3612.
33. Caracciolo, G.; Pozzi, D.; Capriotti, A. L.; Cavaliere, C.; Piovesana, S.; Amenitsch, H.; Laganà, A., Lipid composition: A "key factor" for the rational manipulation of the liposome-protein corona by liposome design. *RSC Advances* **2015,** *5* (8), 5967-5975.
34. Kelly, P. M.; Åberg, C.; Polo, E.; O'Connell, A.; Cookman, J.; Fallon, J.; Krpetić, Ž.; Dawson, K. A., Mapping protein binding sites on the biomolecular corona of nanoparticles. *Nature nanotechnology* **2015,** *10* (5), 472-479.
35. O'Connell, D.; Bombelli, F. B.; Pitek, A.; Monopoli, M.; Cahill, D.; Dawson, K., Characterization of the bionano interface and mapping extrinsic interactions of the corona of nanomaterials. *Nanoscale* **2015,** *7* (37), 15268-15276.
36. Giudice, M. C. L.; Herda, L. M.; Polo, E.; Dawson, K. A., In situ characterization of nanoparticle biomolecular interactions in complex biological media by flow cytometry. *Nature Communications* **2016,** *7*, 13475.
37. Hristov, D. R.; Rocks, L.; Kelly, P. M.; Thomas, S. S.; Pitek, A. S.; Verderio, P.; Mahon, E.; Dawson, K. A., Tuning of nanoparticle biological functionality through controlled surface chemistry and characterisation at the bioconjugated nanoparticle surface. *Scientific reports* **2015,** *5*, 17040.
38. Zhang, X.-Q.; Xu, X.; Bertrand, N.; Pridgen, E.; Swami, A.; Farokhzad, O. C., Interactions of nanomaterials and biological systems: Implications to personalized nanomedicine. *Advanced drug delivery reviews* **2012,** *64* (13), 1363-1384.

39. Mo, Z.-C.; Ren, K.; Liu, X.; Tang, Z.-L.; Yi, G.-H., A high-density lipoprotein-mediated drug delivery system. *Advanced drug delivery reviews* **2016,** *106*, 132-147.
40. Manders, E.; Verbeek, F.; Aten, J., Measurement of co-localization of objects in dual-colour confocal images. *Journal of microscopy* **1993,** *169* (3), 375-382.
41. Bolte, S.; Cordelieres, F., A guided tour into subcellular colocalization analysis in light microscopy. *Journal of microscopy* **2006,** *224* (3), 213-232.
42. Dunn, K. W.; Kamocka, M. M.; McDonald, J. H., A practical guide to evaluating colocalization in biological microscopy. *American Journal of Physiology-Cell Physiology* **2011,** *300* (4), C723-C742.
43. Di Rienzo, C.; Gratton, E.; Beltram, F.; Cardarelli, F., Fast spatiotemporal correlation spectroscopy to determine protein lateral diffusion laws in live cell membranes. *Proceedings of the National Academy of Sciences* **2013,** *110* (30), 12307-12312.
44. Hebert, B.; Costantino, S.; Wiseman, P. W., Spatiotemporal image correlation spectroscopy (STICS) theory, verification, and application to protein velocity mapping in living CHO cells. *Biophysical journal* **2005,** *88* (5), 3601-3614.
45. Barrán-Berdón, A. L.; Pozzi, D.; Caracciolo, G.; Capriotti, A. L.; Caruso, G.; Cavaliere, C.; Riccioli, A.; Palchetti, S.; Laganaì, A., Time evolution of nanoparticle-protein corona in human plasma: Relevance for targeted drug delivery. *Langmuir* **2013,** *29* (21), 6485-6494.

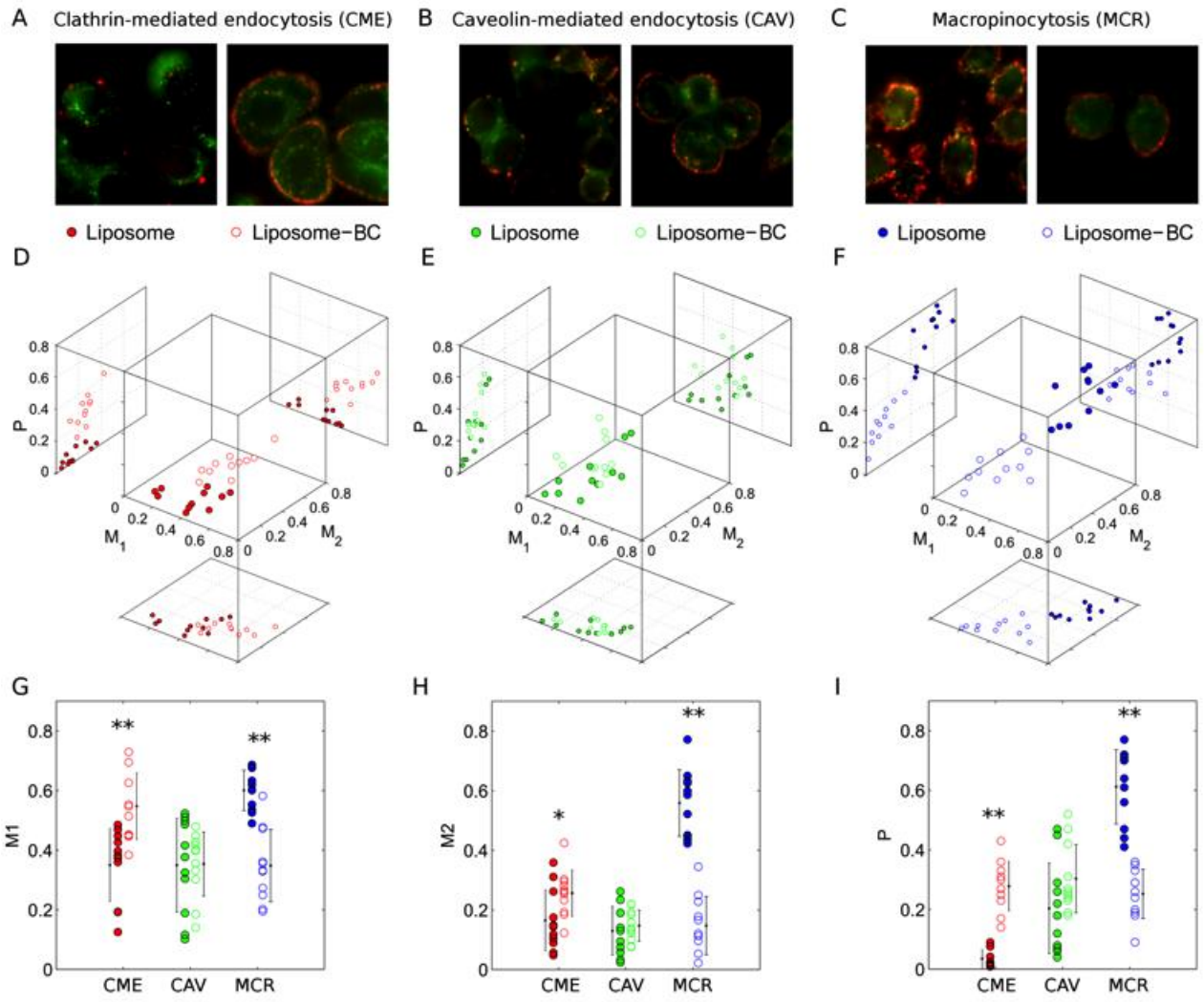

Figure 1. Dual color fluorescence images of red-labeled liposomes, liposome-BC complexes and green-labeled endocytic vesicles corresponding to (A) Clathrin-mediated endocytosis (CME), (B) Caveolin-mediated endocytosis (CAV) CAV and (C) Macropinocytosis (MCR). (D, E, F) Measured values of Manders' (M1, M2) and Pearson's (P) coefficients as multivariate distributions and (G, H, I) corresponding 1D projections. Asterisks refer to Student's t-test significance, in terms of p-values below (*) 0.01 and (**) 0.005.

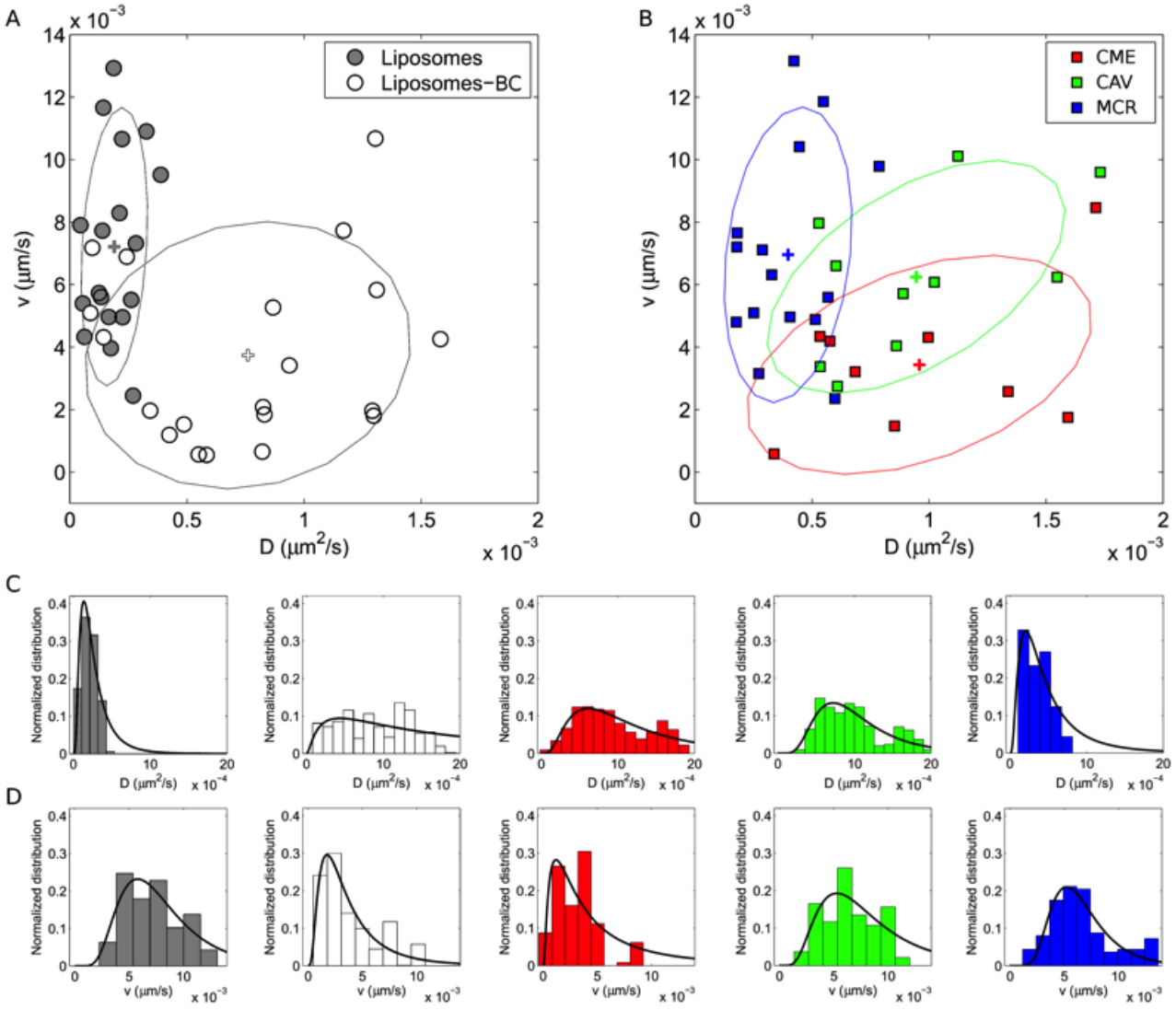

Figure 2. Distributions of the measured dynamic parameters for liposomes and liposome-BC complexes (A) and (B) endocytic vesicles: clathrin-mediated endocytic vesicles (CME), caveolae (CAV) and micropinosomes (MCR). Corresponding weighted distributions of diffusion coefficient, D, and particle speed, v. Crosses indicate the distributions' centroids.

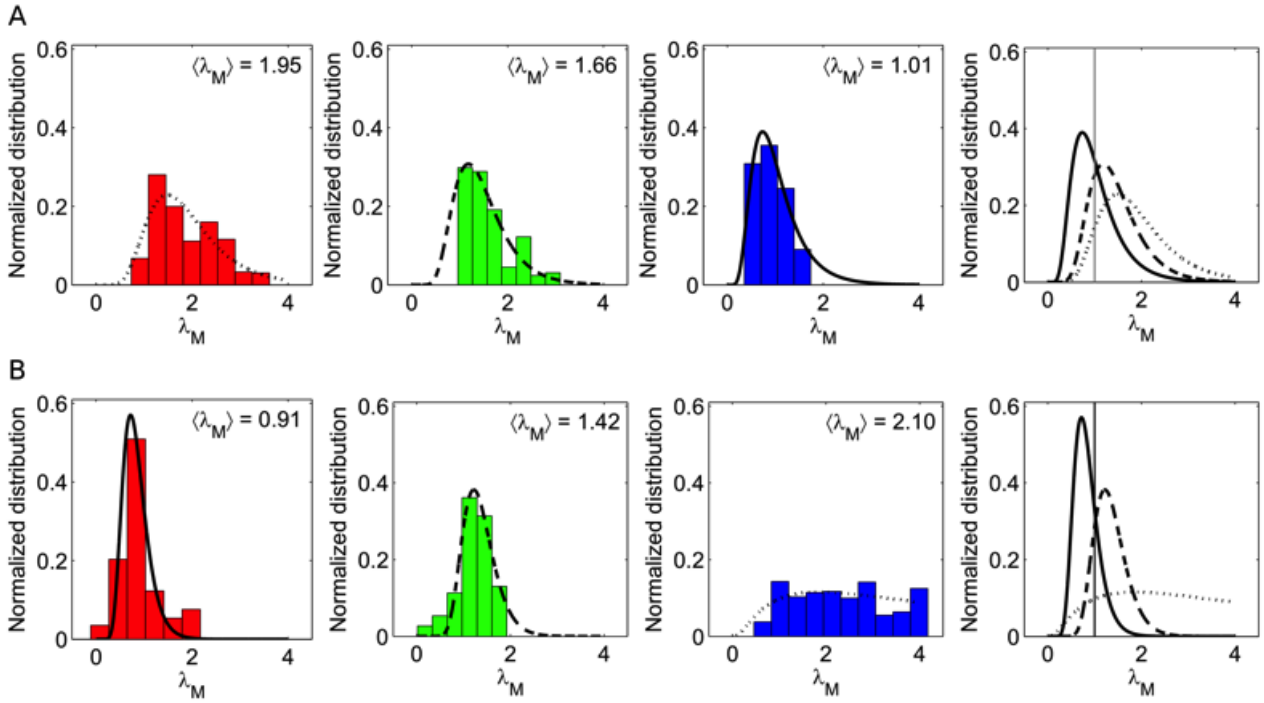

Figure 3. Histograms representing the Mahalanobis distances of data points corresponding to (A) liposomes and (B) liposome-BC complexes, from the distributions of clathrin-mediated endocytic vesicles (red), caveolae (green) and micropinosomes (blue).

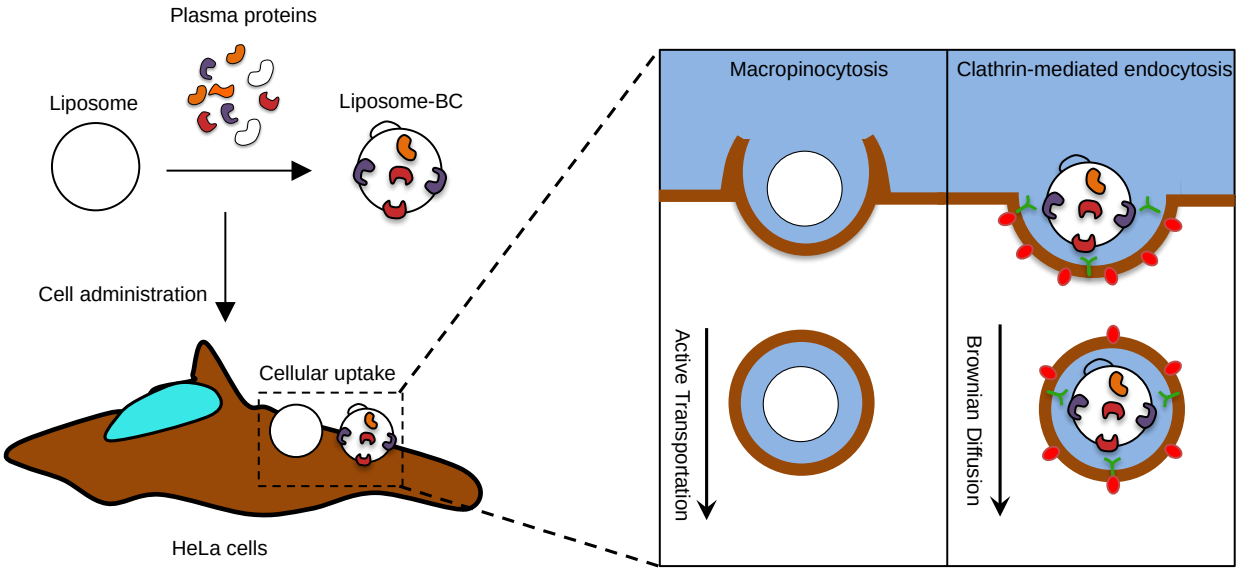

Figure 4. (A) Following exposure to plasma proteins, liposomes' surface is decorated by a biomolecular corona (BC), which depends on several factors such liposome' physiochemical properties (i.e. surface chemistry, size, charge etc.), protein source (e.g. human plasma vs. mouse plasma) and environmental factors (i.e. temperature, pH, etc.). To the sake of clarify, we underline that proteins cover liposome' surface entirely, but, for simplicity of representation, we left the liposome surface only partly decorated by plasma proteins. (B) When particles are given to HeLa cells, they are efficiently internalized with cellular uptake being higher than 90% as quantified by flow cytometry. Despite similar levels of cellular uptake, BC promotes a neat switch of cell entry mechanism of liposomes, from macropinocytosis to clathrin-dependent endocytosis (C). BC has a major impact on the intracellular dynamics of liposomes. Our results highlight the crucial role of BC as an intrinsic trigger of specific NP-cell interactions and biological responses.

Table of Contents